

On the Geometry of Receiver Operating Characteristic and Precision-Recall Curves

Reza Sameni

Department of Biomedical Informatics, Emory University
 Department of Biomedical Engineering, Georgia Institute of Technology
rsameni@dbmi.emory.edu
<https://sameni.info/>

June 13, 2025

Abstract

We study the geometry of Receiver Operating Characteristic (ROC) and Precision-Recall (PR) curves in binary classification problems. The key finding is that many of the most commonly used binary classification metrics are merely functions of the composition function $G := F_p \circ F_n^{-1}$, where $F_p(\cdot)$ and $F_n(\cdot)$ are the class-conditional cumulative distribution functions of the classifier scores in the positive and negative classes, respectively. This geometric perspective facilitates the selection of operating points, understanding the effect of decision thresholds, and comparison between classifiers. It also helps explain how the shapes and geometry of ROC/PR curves reflect classifier behavior, providing objective tools for building classifiers optimized for specific applications with context-specific constraints. We further explore the conditions for classifier dominance, present analytical and numerical examples demonstrating the effects of class separability and variance on ROC and PR geometries, and derive a link between the positive-to-negative class leakage function $G(\cdot)$ and the Kullback–Leibler divergence. The framework highlights practical considerations, such as model calibration, cost-sensitive optimization, and operating point selection under real-world capacity constraints, enabling more informed approaches to classifier deployment and decision-making.

1 Motivation

Classification is a core element in machine learning (ML) and artificial intelligence (AI), with broad applications across science, engineering, and medicine. Classifier performance is typically evaluated using metrics derived from *Receiver Operating Characteristic (ROC)* and *Precision-Recall (PR)* curves. While these metrics are widely used and intuitive, their geometric structure and interrelationships are often overlooked. As a result, threshold selection and performance evaluation are frequently based on heuristics or application-specific constraints, with limited theoretical support.

A geometric view of these curves offers valuable insight. It reveals that metrics such as sensitivity, specificity, precision, and recall are deeply connected through the distributions of classifier scores and class prevalences. This perspective simplifies performance analysis, clarifies the conditions under which classifiers succeed or fail, and supports more principled classifier design and optimization tailored to specific contexts.

Motivated by these insights, we study the geometry of ROC and PR curves. We show that many common binary classification metrics naturally arise from a single composition function linking the score distributions across classes, while others are functions of both class-conditional cumulative distribution functions. This yields a unified geometric framework for understanding classifier behavior, comparing models, and selecting optimal operating points for practical applications.

The hereby presented geometric perspective to ROC and PR curves has been partially explored in the literature. Interested readers are invited to refer to these works for further context and insights [1, 2, 3].

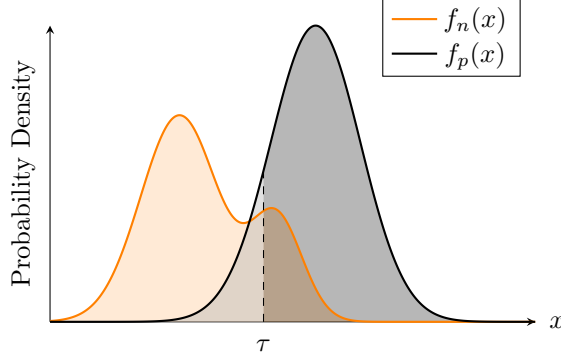


Figure 1: Illustration of score distributions $f_n(x)$ and $f_p(x)$ in a binary classification problem. Shaded regions show classifier decisions based on the threshold τ ; observed score distribution $f(x)$ (pool of both classes) not shown. See (4), (5), (6), and (7) for definitions of shaded areas.

2 Binary Classification Setup

Consider a binary classification problem in which a classifier \mathcal{C} assigns continuous real-valued scores $x \in \mathbb{R}$ to input sample points. These scores represent the classifier’s assessment of how strongly a sample point is associated with either the negative class (c_n) or the positive class (c_p). The scores may or may not have been normalized to represent actual probabilities of association with the two classes (based on a given training set) in general, or calibrated for a given dataset. The objective is to determine whether a given sample point ‘ s ’ belongs to the negative or positive class based on its score. Here, we focus on *pretrained classifiers*, as our interest is in evaluating classification performance and metrics on validation or test data, without delving into the specifics of the model training process. Nonetheless, we use an analytical probabilistic approach, which enables the application of our findings to classifier design.

The score x is (generally) a function of the validation/test sample point s , i.e., $x(s)$. For notational simplicity, we omit the argument s unless explicitly required.

Let $f(x, s)$ denote the joint distribution of scores and sample points for a classifier on a dataset. The score distributions for the evaluated data, conditioned on the negative and positive classes, are denoted by $f_n(x)$ and $f_p(x)$, respectively (see Fig. 1), and are found as follows:

$$\begin{aligned} f_n(x) &:= f(x \mid s \in c_n) = \frac{f(x, s \in c_n)}{\Pr(s \in c_n)} = \frac{f(x, s \in c_n)}{\pi_n}, \\ f_p(x) &:= f(x \mid s \in c_p) = \frac{f(x, s \in c_p)}{\Pr(s \in c_p)} = \frac{f(x, s \in c_p)}{\pi_p}. \end{aligned} \quad (1)$$

Here, $\pi_n := \Pr(s \in c_n)$ and $\pi_p := \Pr(s \in c_p)$ represent the prior probabilities of the negative and positive classes, respectively, and fulfill: $\pi_n + \pi_p = 1$.

The cumulative distribution functions (CDFs) associated with $f_n(x)$ and $f_p(x)$ are shown as shaded areas in Fig. 1:

$$F_n(x) = \int_{-\infty}^x f_n(t) dt, \quad F_p(x) = \int_{-\infty}^x f_p(t) dt. \quad (2)$$

Apparently $F_n(\cdot), F_p(\cdot) : (-\infty, \infty) \rightarrow [0, 1]$.

Our decision rule uses a threshold τ that partitions the score space into two regions: if $x \geq \tau$, the classifier assigns the sample point to class c_p ; otherwise, it assigns the sample point to class c_n :

$$\delta(s) = \begin{cases} c_p, & \text{if } x \geq \tau \\ c_n, & \text{if } x < \tau \end{cases} \quad (3)$$

The choice of threshold τ directly affects the trade-off between false positives and true positives, determining the classifier’s operating point on the ROC or PR curves, and computing confusion matrices.

3 Binary Classification Metrics

Given the score distributions $f_n(x)$ and $f_p(x)$ under the negative and positive classes, respectively, the performance of the classifier at a decision threshold τ can be expressed using standard detection theoretical or ML metrics [4]:

– True Positive Rate (TPR):

$$\text{tpr}(\tau) = \int_{\tau}^{\infty} f_p(x) dx = 1 - F_p(\tau) \quad (4)$$

– True Negative Rate (TNR):

$$\text{tnr}(\tau) = \int_{-\infty}^{\tau} f_n(x) dx = F_n(\tau) \quad (5)$$

– False Positive Rate (FPR):

$$\text{fpr}(\tau) = \int_{\tau}^{\infty} f_n(x) dx = 1 - F_n(\tau) \quad (6)$$

– False Negative Rate (FNR):

$$\text{fnr}(\tau) = \int_{-\infty}^{\tau} f_p(x) dx = F_p(\tau) \quad (7)$$

Equations (4)–(7) quantify how the decision threshold τ partitions the score space into predicted positive and negative classes. They provide the foundation for evaluating standard binary classification performance metrics, such as precision, recall, specificity, and the areas under the ROC and PR curves.

3.1 Finite Sample-Size Approximations

In practice, classifier performance is often evaluated on finite-size datasets. Suppose an evaluation/test set of size T , consisting of P positive and $N = T - P$ negative sample points. In this setting, when we apply the classifier \mathcal{C} to the dataset, the true positive, true negative, false positive, and false negative counts at a given threshold τ are denoted by $\text{TP}(\tau)$, $\text{TN}(\tau)$, $\text{FP}(\tau)$, and $\text{FN}(\tau)$, respectively. These satisfy:

$$\begin{aligned} \text{TP}(\tau) + \text{FN}(\tau) &= P, \\ \text{TN}(\tau) + \text{FP}(\tau) &= N, \\ \text{TP}(\tau) + \text{TN}(\tau) + \text{FP}(\tau) + \text{FN}(\tau) &= T. \end{aligned} \quad (8)$$

Using (8), the performance metrics and class prior probabilities can be approximated as:

$$\begin{aligned} \text{tpr}(\tau) &\approx \frac{\text{TP}(\tau)}{P}, & \text{fpr}(\tau) &= 1 - \text{tnr}(\tau) \approx \frac{\text{FP}(\tau)}{N}, \\ \text{tnr}(\tau) &\approx \frac{\text{TN}(\tau)}{N}, & \text{fnr}(\tau) &= 1 - \text{tpr}(\tau) \approx \frac{\text{FN}(\tau)}{P}, \\ \pi_p &\approx \frac{P}{T}, & \pi_n &= 1 - \pi_p \approx \frac{N}{T}. \end{aligned} \quad (9)$$

These empirical approximations converge to their distribution-based counterparts as $T \rightarrow \infty$, under the assumption that samples are independently drawn from the underlying score distributions $f_n(x)$ and $f_p(x)$.

The most common classification evaluation measures are summarized in Fig. 2. Note that when a trained classifier is applied to an evaluation or test dataset with fixed values of P and N , the resulting confusion matrix is fully determined by the decision threshold. Therefore, despite the diversity of evaluation metrics, a given binary classifier has only a single degree of freedom at inference time—defined by the choice of its decision threshold.

Confusion Matrix		
	Predicted +	Predicted –
Actual +	TP	FN
Actual –	FP	TN

Common Evaluation Metrics		
$\text{TPR (Sensitivity or Recall)} = \frac{TP}{TP + FN}$		
$\text{TNR (Specificity)} = \frac{TN}{TN + FP}$		
$\text{FPR} = \frac{FP}{FP + TN} = 1 - \text{Specificity}$		
$\text{FNR} = \frac{FN}{TP + FN} = 1 - \text{Sensitivity}$		
$\text{Accuracy} = \frac{TP + TN}{TP + TN + FP + FN}$		
$\text{PPV (Precision)} = \frac{TP}{TP + FP}$		
$\text{NPV} = \frac{TN}{TN + FN}$		
$\text{F}_\beta\text{-score} = (1 + \beta^2) \frac{\text{Precision} \times \text{Recall}}{(\beta^2 \times \text{Precision}) + \text{Recall}}$		

Figure 2: Common classification evaluation measures

3.2 $G = (F_p \circ F_n^{-1})$ — Positive-to-Negative Class Leakage Function

For any $u \in [0, 1]$, $F_n^{-1}(u)$ is a mapping from the negative class probability space back to the score space. In other words, $F_n^{-1}(u)$ provides the score t at which the probability of observing scores given to sample points from class c_n is u (i.e., a fraction u of the negative class distribution lies below t). Therefore, applying F_p to this same threshold—i.e., evaluating $F_p(F_n^{-1}(u))$ —answers the question: “Given the threshold where u proportion of scores assigned to negatives lie below, how likely is it that a score assigned to a sample point from the positive class also falls below this same threshold (resulting in its misclassification)?” A good classifier would make this probability negligible, so that a threshold accommodating a certain portion of negatives does not include too many positives. With this insight, we define

$$G(u) := F_p(F_n^{-1}(u)) = (F_p \circ F_n^{-1})(u), \quad (10)$$

as a *positive-to-negative class leakage function*, since it measures how much the negative threshold at level u encroaches upon the positive distribution. $G(\cdot)$ is a monotonic mapping between two probability spaces: $G(\cdot) : [0, 1] \rightarrow [0, 1]$ and it fulfills $G(0) = 0$ and $G(1) = 1$ with a probability density function:

$$g(u) := \frac{d}{du} G(u) \quad (11)$$

Intuitively, the more $f_n(\cdot)$ and $f_p(\cdot)$ overlap, the larger the area under $G(\cdot)$ becomes, indicating that many positive sample points are scored below a threshold chosen for negatives. We will provide supporting evidence for this property in Section 4.2.

4 Classifier Evaluation Measures

4.1 Receiver Operating Characteristic (ROC) Curve

The Receiver Operating Characteristic (ROC) curve is a graphical representation showing TPR (i.e., *sensitivity*, or $1 - \text{miss-rate}$) against FPR (i.e., $1 - \text{specificity}$), illustrating the trade-offs between false positives and true positives as the decision threshold τ varies [1].

According to (4) and (6), TPR and FPR are monotonic functions of τ . Therefore, each threshold τ corresponds to unique TPR and FPR values:

$$\tau = F_p^{-1}(1 - \text{tpr}(\tau)) = F_n^{-1}(1 - \text{fpr}(\tau)), \quad (12)$$

which results in $\text{tpr}(\tau) = 1 - (F_p \circ F_n^{-1})(1 - \text{fpr}(\tau))$ providing a compact formulation of the ROC curve [1, Sec 2.2.4]:

$$\boxed{\text{tpr}(\tau) = 1 - G(1 - \text{fpr}(\tau))} \quad (13)$$

parameterized by the decision threshold τ . From (13), the monotonically increasing shape of the ROC curve is apparent. It also leads to the following results:

$$\text{miss-rate}(\tau) = 1 - \text{tpr}(\tau) = G(\text{specificity}(\tau)), \quad (14)$$

$$\text{fpr}(\tau) = 1 - G^{-1}(1 - \text{tpr}(\tau)). \quad (15)$$

A practically important implication of (13) is that as long as F_p and F_n are well-learned from the training data (or known/presumed a priori), the shape of the ROC curve is not impacted by the positive vs. negative class prevalence in the validation/test sets. We will later show that this is not the case for the PR curve.

4.2 Area Under the ROC Curve (AUROC)

The AUROC follows directly from the ROC geometry derived in (13), where the AUROC is the area under this curve:

$$\text{AUROC} = \int_0^1 \text{tpr}(u) du = \int_0^1 [1 - (F_p \circ F_n^{-1})(1 - u)] du. \quad (16)$$

With a change of variable $v = 1 - u$ and $du = -dv$, this becomes:

$$\text{AUROC} = \int_1^0 [1 - G(v)] (-dv) = 1 - \int_0^1 G(v) dv. \quad (17)$$

This shows that AUROC is fully determined by the composition of the class-conditional score distribution CDFs. The further $G(\cdot)$ lies below the identity line, the higher the AUROC value—indicating stronger class separation. In other words, maximizing AUROC requires minimizing the area under the non-negative curve of $G(\cdot)$.

Alternative Interpretation: Equation (17) aligns with the interpretation of AUROC as the probability that a randomly chosen positive sample point ranks higher than a randomly chosen negative one. In other words, as shown in the Appendix [5, 6]:

$$\text{AUROC} = \Pr(x_p > x_n) = \int_{-\infty}^{\infty} f_p(x) F_n(x) dx = \int_{-\infty}^{\infty} \dot{F}_p(x) F_n(x) dx \quad (18)$$

where $x_p \sim f_p(x)$ is a score randomly drawn from the positive class distribution, and $x_n \sim f_n(x)$ is a score randomly drawn from the negative class distribution. The two are assumed to be independent. Combining (17) and (18) yields

$$\Pr(x_n \geq x_p) = \int_0^1 G(v) dv \quad (19)$$

which is an area that an ideal classifier seeks to minimize.

A typical ROC curve with the highlighted AUROC and the composition function $G(\cdot)$ is shown in Fig. 3. In Appendix B, we further relate $G(\cdot)$ with the Kullback–Leibler divergence between the class score density functions f_p and f_n .

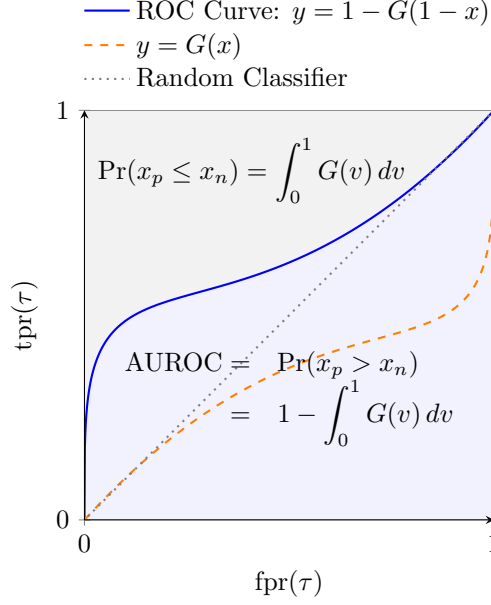


Figure 3: A typical ROC curve highlighting the composition function $G(\cdot)$ and the AUROC.

4.3 Precision-Recall (PR) Curve

The PR curve shows precision, or the positive predictive value (PPV), vs. recall (sensitivity or TPR) [7], illustrating the potential trade-offs between the accuracy of positive predictions and the ability to detect positive cases as the decision threshold τ varies.

Probabilistically, PPV at threshold τ is $\Pr(s \in c_p \mid x > \tau)$, which can be expressed in terms of the TPR, score distributions and class priors:

$$\begin{aligned}
 \text{ppv}(\tau) &= \frac{\Pr(x > \tau \mid s \in c_p) \cdot \Pr(s \in c_p)}{\Pr(x > \tau)} \\
 &= \frac{\pi_p \int_{\tau}^{\infty} f_p(x) dx}{\pi_p \int_{\tau}^{\infty} f_p(x) dx + \pi_n \int_{\tau}^{\infty} f_n(x) dx} \\
 &= \frac{\pi_p \cdot [1 - F_p(\tau)]}{\pi_p \cdot [1 - F_p(\tau)] + \pi_n \cdot [1 - F_n(\tau)]} \\
 &= \frac{\pi_p \cdot \text{tpr}(\tau)}{\pi_p \cdot \text{tpr}(\tau) + \pi_n \cdot \text{fpr}(\tau)} = \frac{1}{1 + \frac{\pi_n}{\pi_p} \cdot \frac{\text{fpr}(\tau)}{\text{tpr}(\tau)}} \\
 &= \frac{\text{tpr}(\tau)}{\text{tpr}(\tau) + \frac{\pi_n}{\pi_p} \cdot [1 - (F_n \circ F_p^{-1})(1 - \text{tpr}(\tau))]}
 \end{aligned} \tag{20}$$

Therefore

$$\boxed{\text{ppv}(\tau) = \frac{\text{tpr}(\tau)}{\text{tpr}(\tau) + \frac{\pi_n}{\pi_p} \cdot [1 - G^{-1}(1 - \text{tpr}(\tau))]} } \tag{21}$$

Accordingly, precision and PR depend not only on the classifier's score distributions but also on the class prior probabilities in the dataset. As compared with the ROC curve, it is also a more complex function of $G(\cdot)$.

4.4 Accuracy

The accuracy of a binary classifier at decision threshold τ is the probability of correct classification, computed as the weighted sum of the true positive and true negative rates (cf. Fig. 2 for the finite-sample approximation):

$$\text{Accuracy}(\tau) = \pi_p \cdot \text{tpr}(\tau) + \pi_n \cdot \text{tnr}(\tau) = \pi_p \cdot [1 - F_p(\tau)] + \pi_n \cdot F_n(\tau) \quad (22)$$

This shows that accuracy depends on the class priors π_n and π_p , as well as the CDFs of the classifier scores under the positive and negative classes. Apparently, accuracy is not only a function of the composition $G(\cdot)$ but rather a function of both F_n and F_p .

4.5 F_β Score — A Generalized Harmonic Metric

The F_β score is a generalization of the F_1 score that provides a tunable trade-off between precision and recall. It is the weighted harmonic mean of precision (positive predictive value) and recall (TPR or sensitivity, cf. Fig. 2):

$$F_\beta = (1 + \beta^2) \cdot \frac{\text{Precision} \cdot \text{Recall}}{(\beta^2 \cdot \text{Precision}) + \text{Recall}} \quad (23)$$

The parameter $\beta > 0$ controls the balance:

- $\beta = 1$ yields the standard F_1 score, equally weighting precision and recall.
- $\beta > 1$ emphasizes recall (sensitivity) more heavily than precision.
- $\beta < 1$ emphasizes precision over recall.

To relate the F_β score to the score distributions and the class priors, we use:

$$\text{Precision}(\tau) = \frac{\pi_p \cdot \text{tpr}(\tau)}{\pi_p \cdot \text{tpr}(\tau) + \pi_n \cdot \text{fpr}(\tau)}, \quad \text{Recall}(\tau) = \text{tpr}(\tau) \quad (24)$$

Substituting into the F_β formula yields:

$$F_\beta(\tau) = \frac{(1 + \beta^2) \cdot \text{tpr}(\tau)}{\text{tpr}(\tau) + \beta^2 + \beta^2 \cdot \frac{\pi_n}{\pi_p} \cdot \frac{\text{fpr}(\tau)}{\text{tpr}(\tau)}} \quad (25)$$

Next, using the definitions of $\text{tpr}(\tau)$ and $\text{fpr}(\tau)$, (25) can be rewritten as:

$$F_\beta(\tau) = \frac{(1 + \beta^2)(1 - F_p(\tau))}{(1 - F_p(\tau)) + \beta^2 \left[1 + \frac{\pi_n}{\pi_p} \cdot \frac{1 - F_n(\tau)}{1 - F_p(\tau)} \right]} \quad (26)$$

This shows how F_β depends on the threshold τ , the class priors π_n/π_p , and the score distributions $F_n(\tau)$ and $F_p(\tau)$. Larger values of $1 - F_p(\tau)$ (true positives) improve F_β , while higher $1 - F_n(\tau)$ (false positives) and stronger class imbalance degrade it—especially when β emphasizes recall. Similar to accuracy, $F_\beta(\tau)$ is a function of both $F_n(\cdot)$ and $F_p(\cdot)$, not just the composite $G(\cdot)$.

5 Dominating Classifiers

Suppose we have classifiers \mathcal{C}_1 and \mathcal{C}_2 with positive-to-negative class leakage functions $G_1(\cdot)$ and $G_2(\cdot)$, respectively. We say that \mathcal{C}_1 dominates \mathcal{C}_2 if the ROC and PR curves of \mathcal{C}_1 lie entirely on or above those of \mathcal{C}_2 . That is, \mathcal{C}_1 achieves sensitivity (TPR) greater than that of \mathcal{C}_2 at all false positive rates (FPR), and precision greater than that of \mathcal{C}_2 at all recall levels. We refer to this case as *global dominance*. In contrast, if

\mathcal{C}_1 only outperforms \mathcal{C}_2 over a subset of the domain—e.g., at certain FPR ranges or specific recall intervals—we say that \mathcal{C}_1 has *local dominance* over \mathcal{C}_2 . From (13) and (21), it follows that for both ROC and PR curves local dominance holds whenever, for a given u ,

$$G_1(u) < G_2(u) \quad (27)$$

and global dominance holds when the above holds for all $u \in [0, 1]$. We further name the dominance *non-strict* if $G_1(u) \leq G_2(u)$. Importantly,

- When the ROC or PR curve of \mathcal{C}_1 globally dominates that of \mathcal{C}_2 , the corresponding PR or ROC curve is also guaranteed to be globally dominated (since the dominance holds for all $u \in [0, 1]$). However, if the dominance is only local, there is no such guarantee— \mathcal{C}_1 may outperform \mathcal{C}_2 in specific segments of the curves.
- Even if a classifier globally or locally dominates another in terms of both ROC and PR curves, there is no guarantee that it also dominates in measures such as accuracy and F_β , which depend on both $F_p(\cdot)$ and $F_n(\cdot)$, not merely on $G_1(\cdot)$ and $G_2(\cdot)$. In fact, two classifiers can have identical ROC/PR curves but different accuracies or F_β scores.
- Classification evaluation metrics are statistical aggregations over a population of sample points and do not provide much information about specific sample points or subpopulations. Therefore, in heterogeneous datasets, a classifier that generally underperforms across the full population might still perform well on specific subpopulations, and a classifier that strictly dominates other classifiers may still underperform on specific subgroups.
- Even a weak classifier that performs well only on specific subgroups can be beneficial in ensemble methods such as voting or boosting, which combine the strengths of multiple classifiers to improve overall performance.

6 Design Constraints and Operating Point Selection

Classification is inherently probabilistic, and no practical classifier is ever perfect (unless for trivial classification problems). Therefore, false positives and negative cases are inevitable and depending on the chosen score threshold, different trade-offs arise. Although classifiers are often designed and compared using abstract metrics such as AUROC, accuracy, or F_β score, real-world constraints can dictate the operating point—that is, the threshold at which a model labels an instance positively or negatively.

In the following, we explore practical scenarios, illustrating how real-world constraints guide the selection of the operating point. The studied cases and the ROC plane design regions corresponding to each case are illustrated in Fig. 4.

6.1 Limited/Fixed Capacity of Admitting Positive Cases

In real-world scenarios, AI- or machine-learning-powered tools are often integrated into existing human-centric workflows. For example, if a classifier is used for prescreening patients for a specific medical condition, the positively classified cases are typically referred to a physician or a lab test. However, healthcare facilities usually do not have the capacity to accommodate all referrals. They are constrained by the number of available physicians—whether on duty or on call—as well as hospital beds, lab testing capacity and other factors. On the other hand, under-referral (i.e., too few positive referrals) is another undesired scenario that can result in missed diagnoses, delayed treatments, and potential harm to patients, ultimately compromising clinical outcomes and leading to unjustifiable operational costs for a healthcare system.

As a result, there is often a hard or soft limit on the maximum (or even minimum) number of positive cases beyond which the healthcare system cannot admit additional patients. For example, for the maximum, the sum of the true and false positives may be capped, i.e., $TP + FP \leq M$, where M is “the maximum number of cases that the classifier can label as positive while remaining within the healthcare system’s capacity for patient admission ($M \leq P$).” Importantly, these capacities and limitations are dynamic and vary over time

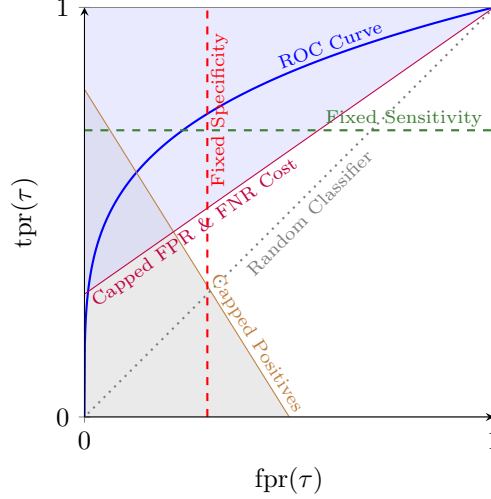


Figure 4: Illustration of different constrained scenarios and the corresponding design regions in the ROC plane.

and setting, making the problem more complicated. Similar constraints arise in other application domains as well.

Note that in the scenario described above, M may or may not scale with the total number of subjects (T). For example, in an overwhelmed healthcare setting operating at maximum capacity, M may not scale easily with an increase in the number of patients (T). Defining $m := M/T$, as the *maximum admission rate* and using (9), we obtain:

$$\pi_p \text{tpr}(\tau) + \pi_n \text{fpr}(\tau) \leq m \quad (28)$$

In the ROC plane, (28) describes a triangular region below a line with negative slope $-\pi_n/\pi_p = -N/P$, intersecting the TPR (vertical) axis at $m/\pi_p = M/P$ and the FPR (horizontal) axis at $m/\pi_n = M/N$, as shown in Fig. 4. Apparently feasible operating points of the classifier must lie within or below this region to satisfy the capacity constraint. In this scenario, the “optimal” operating point on the ROC curve would be the intersection of the ROC curve with the line in (28). The y -intercept and the optimal operating point (and the decision threshold τ), will generally change based on T . See [8] for a practical application in prescreening Chagas disease, where this classification setting was explored.

6.2 Bounded Risk Classification

False positives and false negatives are both costly. False positives impose operational costs, require excess human (expert) interventions, and may lead to a loss of trust in AI-supported systems. False negatives may result in delayed or missed treatments, and other critical failures. While we ideally seek to minimize both, as discussed in previous sections, there is always a trade-off. In practice, this trade-off can be formulated as a risk analysis problem aiming to minimize a weighted cost of false positives and false negatives.

Assuming the risk is modeled as a linear combination of false negatives and false positives, we seek to satisfy the constraint $\alpha \text{FP} + \beta \text{FN} \leq C$, where C is the maximum allowable cost, and α and β are the cost factors associated with false positives and false negatives, respectively. Using (9), this constraint can be rewritten as $\alpha N \text{fpr}(\tau) + \beta P \text{fpr}(\tau) \leq C$, or, in terms of the ROC variables:

$$\alpha \pi_n \text{fpr}(\tau) + \beta \pi_p (1 - \text{tpr}(\tau)) \leq c \quad (29)$$

where $c := C/T$ is the population-size normalized cost. As shown in Fig. 4, in the ROC space, (29) defines a region above a line with positive slope $(\alpha \pi_n)/(\beta \pi_p)$ and y -intercept $1 - c/(\beta \pi_p)$.

6.3 Cost-Aware Multiobjective Classification

Another practical scenario is the case where a real-world socioeconomic cost is associated to the false positives and negatives. Missing a positive case may result in significant downstream consequences—such as a delayed diagnosis in healthcare, which could lead to disease progression, higher treatment costs, and in some cases, irreversible harm or death. These outcomes can not only impact the patient but also result in financial liabilities for the hospital, regulatory penalties, and reputational damage. On the other hand, a false positive may lead to unnecessary follow-up procedures, increased workload for clinicians, patient anxiety, and inflated operational costs. In sectors like finance or insurance, false negatives might mean undetected fraud, while false positives could flag legitimate customers, affecting user trust and potentially leading to lawsuits.

These real-world costs, though difficult to quantify precisely, highlight the need for explicitly modeling the trade-offs between model performance and annotation cost. One way to address this is to quantify and integrate ML-based design metrics and socioeconomic factors into bi-objective or multiobjective optimization frameworks. For example, in classifier design one could maximize a cost function such as

$$C = (1 - \lambda) \times \text{performance} + \lambda \times (1 - \text{cost}), \quad (30)$$

where “performance” corresponds to any of the typical ML design metrics such as AUROC, accuracy, F_β score, etc., $\text{cost} \in [0, 1]$ is a quantification of the socioeconomic costs of false positive or negative cases, and λ is a regularization parameter. The result of such a bi-objective optimization process is a set of solutions that form what is known as the *Pareto front* [9, 10]—a curve or surface representing the set of models for which no objective (e.g., performance or cost) can be improved without degrading the other. Each point on the Pareto front corresponds to a different trade-off between annotation or socioeconomic cost and predictive performance. This enables stakeholders to make principled decisions about model selection based on their operational constraints or risk tolerance. For instance, a healthcare provider might prioritize minimizing false negatives due to their clinical consequences, while an insurance company might select a model that optimally balances detection of fraudulent claims against the customer experience or potential lawsuits. Such multiobjective ML design landscapes have been explored in the applied ML literature [11, 12, 10].

In multiclass classification problems, the cost of false labels can vary across classes because some diagnoses have similar downstream actions. For example, misclassifying one benign cardiac arrhythmia as another may have little clinical consequence, whereas confusing a life-threatening condition like ventricular tachycardia with a benign rhythm could result in delayed treatment and serious harm to the patient [13]. In such cases, the cost becomes a class-dependent matrix, and the optimization must account for asymmetric risks, further reinforcing the significance of cost-sensitive and multiobjective learning approaches in real-world classifier deployments.

7 Model Calibration

Although we have focused on discrimination metrics such as ROC and PR, many real-world applications require that a classifier’s scores be interpreted as probabilities or likelihoods. For example, given a specific phenotype (feature, measurement) observed from an individual (sample point), what is the probability that the sample point belongs to the positive or negative class? The process of mapping scores to actual probabilities is known as *calibration*.

For instance, if a classifier assigns a sample point s a score $x(s) \approx 0.7$, then ideally, among all points assigned similar scores, approximately 70% should belong to the positive class. This reflects proper calibration, where the output scores can be interpreted as probabilities. In practice, proper calibration is a long-term process that may be performed after a model is deployed and evaluated on large real-world data with confirmed outcomes. It can be assessed using reliability diagrams or proper scoring rules (e.g., Brier score or log loss) that compare predicted probabilities against empirical frequencies. If $x(s)$ is not inherently calibrated, post-hoc techniques such as isotonic regression or Platt scaling can adjust the raw outputs without retraining the classifier. Even a model with favorable ROC or PR characteristics may still require calibration to ensure its score outputs reflect true class probabilities in practical settings.

8 Case Studies

8.1 A Random Classifier

A trivial corner case for (13) is when $f_n(\cdot) = f_p(\cdot)$, i.e., the distribution of the score is not affected by the sample point's class label. We can think of this as a degenerate case where the classifier is unable to distinguish between the two classes. Therefore, $F_n(\cdot) = F_p(\cdot)$ (or $G(\cdot)$ is the identity function), and (13) simplifies to

$$\text{tpr}(\tau) = \text{fpr}(\tau) \quad (31)$$

which corresponds to the ROC curve of a random classifier.

More generally, we can seek conditions for which the classifier performs better than chance, i.e., $\text{tpr}(\tau) > \text{fpr}(\tau)$, or using (13)

$$\text{tpr}(\tau) = 1 - G(1 - \text{fpr}(\tau)) > \text{fpr}(\tau) \quad (32)$$

Considering that $0 \leq \text{tpr}(\tau), \text{fpr}(\tau) \leq 1$, and $G(\cdot)$ is monotonically increasing, $G^{-1}(\cdot)$ is also monotonically increasing and (32) simplifies to $x > G(x)$, or equivalently $G^{-1}(x) > x$.

8.2 An Ideal Classifier

Perfect classification can be achieved when the score distributions under the negative and positive classes are entirely non-overlapping, i.e., there exists at least one decision threshold τ that places all negative sample points strictly below τ and all positive sample points strictly above it (or vice versa). Suppose $f_n(x)$ is supported only in the interval $(-\infty, \tau^*)$ and $f_p(x)$ is supported only in $[\tau^*, \infty)$. Then for any threshold τ in the open interval $(\max \text{supp}(f_n), \min \text{supp}(f_p))$:

$$\text{fpr}(\tau) = \int_{\tau}^{\infty} f_n(x) dx = 0, \quad \text{tpr}(\tau) = \int_{\tau}^{\infty} f_p(x) dx = 1. \quad (33)$$

Hence, the ROC curve immediately jumps from the point $(\text{fpr}(\tau^*) = 0, \text{tpr}(\tau) = 0)$ to $(\text{fpr}(\tau^*) = 0, \text{tpr}(\tau^*) = 1)$, then remains at $\text{tpr}(\tau^*) = 1$ up to $\text{fpr}(\tau^*) = 1$ at the extreme right end of the ROC horizontal axis. This results in AUROC = 1. In other words, no positive sample points ever leak into the negative side for any threshold above $(-\infty, \tau^*)$, and no negative sample points appear above τ^* , achieving both zero false positives and zero false negatives. Equivalently, in terms of the leakage function $G(u) = F_p \circ F_n^{-1}(u)$, since $F_n^{-1}(u) < \tau^*$ for all $u \in [0, 1]$, we have $G(u) = 0$ for all $u \in [0, 1]$. Consequently, from (17) we have

$$\int_0^1 G(u) du = 0 \quad \Rightarrow \quad \text{AUROC} = 1. \quad (34)$$

This represents the ideal yet rare case in which the classifier's scores admit "perfect" separation between the negative and positive classes. In almost all practical problems, f_n and f_p exhibit at least some degree of overlap, so the perfect-classifier scenario does not occur.

8.3 Classifiers with Binormal Distribution Scores

Consider the case where the classifier score distributions under the negative and positive classes are each Gaussian but with different means and variances [1, Sec 2.5]:

$$f_n(x) = \mathcal{N}(x; \mu_n, \sigma_n^2), \quad f_p(x) = \mathcal{N}(x; \mu_p, \sigma_p^2), \quad (35)$$

with corresponding CDFs

$$F_n(x) = \Phi\left(\frac{x - \mu_n}{\sigma_n}\right), \quad F_p(x) = \Phi\left(\frac{x - \mu_p}{\sigma_p}\right), \quad (36)$$

where $\Phi(\cdot)$ is the standard normal CDF, with zero mean and unit standard deviation [14]:

$$\Phi(z) = \frac{1}{\sqrt{2\pi}} \int_{-\infty}^z \exp\left(-\frac{t^2}{2}\right) dt. \quad (37)$$

8.3.1 Parametric Form of the ROC Curve

From (6)–(4), the ROC curve is given by $(\text{fpr}(\tau), \text{tpr}(\tau))$ as τ varies:

$$\begin{aligned}\text{fpr}(\tau) &= 1 - F_n(\tau) = 1 - \Phi\left(\frac{\tau - \mu_n}{\sigma_n}\right), \\ \text{tpr}(\tau) &= 1 - F_p(\tau) = 1 - \Phi\left(\frac{\tau - \mu_p}{\sigma_p}\right).\end{aligned}\tag{38}$$

Eliminating τ yields a convenient parametric form of the ROC curve. Letting $u = (\tau - \mu_n)/\sigma_n$ we obtain

$$\text{fpr}(u) = 1 - \Phi(u), \quad \text{tpr}(u) = 1 - \Phi(\alpha u - b),\tag{39}$$

where

$$\alpha := \sigma_n/\sigma_p, \quad b := (\mu_p - \mu_n)/\sigma_p.\tag{40}$$

Hence the ROC curve can be parameterized as

$$\text{ROC}(u): \quad (\text{fpr}(u), \text{tpr}(u)) = (1 - \Phi(u), 1 - \Phi(\alpha u - b)), \quad u \in (-\infty, \infty).\tag{41}$$

8.3.2 Analytical Expression for the Leakage Function $G(\cdot)$

The inverse CDF of $F_n(\cdot)$ is:

$$F_n^{-1}(u) = \mu_n + \sigma_n \Phi^{-1}(u).\tag{42}$$

Therefore,

$$\begin{aligned}G(u) &= F_p(F_n^{-1}(u)) = \Phi\left(\frac{F_n^{-1}(u) - \mu_p}{\sigma_p}\right) \\ &= \Phi\left(\frac{\mu_n + \sigma_n \Phi^{-1}(u) - \mu_p}{\sigma_p}\right) = \Phi(\alpha \Phi^{-1}(u) - b),\end{aligned}\tag{43}$$

Thus for two Gaussian score distributions, the function $G(u)$ is simply a composition of standard normal CDFs and their inverses. Its shape is fully determined by the ratio between the standard deviations (α) and the normalized gap between their means (b). It is apparent that gaussian distributions with farther mean values and smaller standard deviations result in lower inter-class leakage.

8.3.3 Analytical AUROC Expression

Finally, using (18), since the difference $x_p - x_n$ is normally distributed with $x_p - x_n \sim \mathcal{N}(\mu_p - \mu_n, \sigma_n^2 + \sigma_p^2)$, one obtains [1, Sec 2.5]:

$$\text{AUROC} = \Phi\left(\frac{\mu_p - \mu_n}{\sqrt{\sigma_n^2 + \sigma_p^2}}\right),\tag{44}$$

which according to (17) and (43) is non-evidently one minus the area under $\Phi(\alpha \Phi^{-1}(u) - b)$.

This example confirms that as the separation $(\mu_p - \mu_n)$ grows and/or the spread $(\sigma_n^2 + \sigma_p^2)$ shrinks, the AUROC increases and the classifier becomes more discriminative. By contrast, when $\mu_p = \mu_n$, the AUROC degenerates to 0.5, or a random classifier explained in Section 8.1.

Numeric Examples: To study the impact of score distribution parameters on ROC geometry, we conduct three sets of experiments using Gaussian-distributed scores. In the first experiment (Fig. 5a), the variance ratio is fixed at $\alpha = 1.0$ while the normalized mean separation b is varied across $\{0.0, 1.0, 2.0, 3.0\}$. This setup isolates the effect of increasing class separation on ROC performance. In the second experiment (Fig. 5b), the mean separation is fixed at $b = 0.8$ and α is varied across $\{0.5, 1.0, 1.5, 2.0\}$ to examine the influence of score dispersion between classes. In the third case (Fig. 5c), both α and b are varied to study their

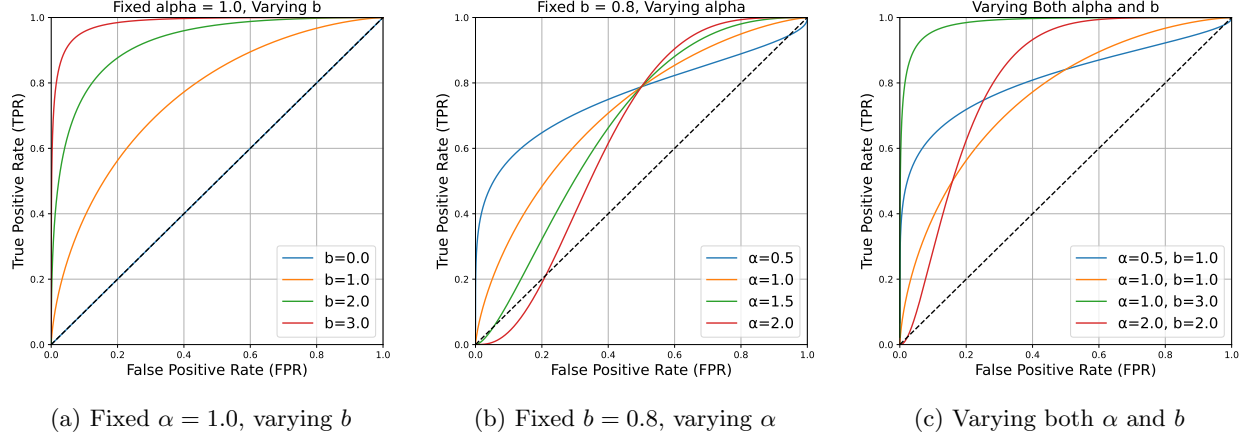


Figure 5: ROC curves for Gaussian score classifiers under different parameter settings. (a) Varying b with fixed α ; (b) Varying α with fixed b ; (c) Joint variation of both parameters.

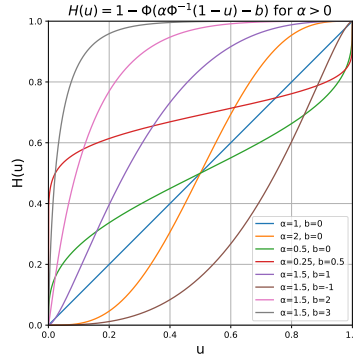


Figure 6: Generic ROC family generated from the transformation $H(u) = 1 - \Phi(\alpha\Phi^{-1}(1-u) - b)$ using different values of $\alpha = \sigma_n/\sigma_p > 0$ and $b = (\mu_p - \mu_n)/\sigma_p$. When $\alpha = 1$ and $b = 0$, the function reduces to the identity line (random classifier). As α increases, the curves become steeper, representing classifiers with more confident separation between positive-negative classes. Increasing b helps improve separability of the two classes. Negative b implies that the class labels or decision rule should be switched (positive class being assigned to lower thresholds).

combined effect on classifier discriminability. All plots exhibit the expected trends: increasing b enhances ROC performance, while deviations in α modulate the steepness and shape of the curves, reflecting changes in overlap between the class-conditional score distributions.

Fig. 6 shows generic ROC curves corresponding to two-Gaussian distributed scores, generated using the expression $H(u) = 1 - \Phi(\alpha\Phi^{-1}(1-u) - b)$, which results from combining (13) and (43). Each curve corresponds to a different combination of (α, b) , demonstrating the impact of the Gaussian distribution parameters on the ROC shape. When $\alpha = 1$ and $b = 0$, the function reduces to the identity line, corresponding to a random classifier. As α increases, the curves become steeper, representing classifiers with more confident separation between positive-negative classes. Shifting b to positive or negative values translates the curve right or left, respectively, modifying the threshold at which positive predictions occur.

To complement the ROC analysis, we conduct three sets of experiments to explore how class prevalence influences the shape and behavior of PR curves. In all cases, the score distributions are modeled as Gaussians with varying mean and variance parameters, described above. Unlike ROC curves, PR curves are sensitive to class imbalance. Therefore, our experiments vary the positive-to-negative class prevalence ratios at $\pi_p = \{0.2, 0.1, 0.3\}$ to study this dependency. In the first scenario (Fig. 7a), the variance ratio is fixed at $\alpha = 1.0$, while the mean separation b varies over $\{0.0, 1.0, 2.0, 3.0\}$. The second experiment (Fig. 7b) fixes $b = 0.8$

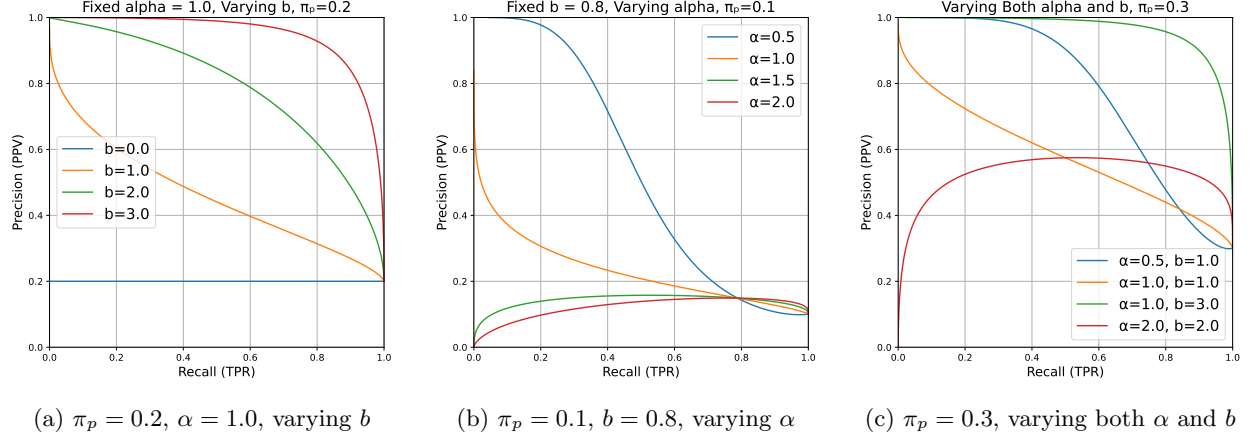


Figure 7: PR curves for binomial positive and negative class scores under varying classifier parameters and class prevalence ratios. Lower π_p/π_n ratios result in reduced precision, despite similar recall performance.

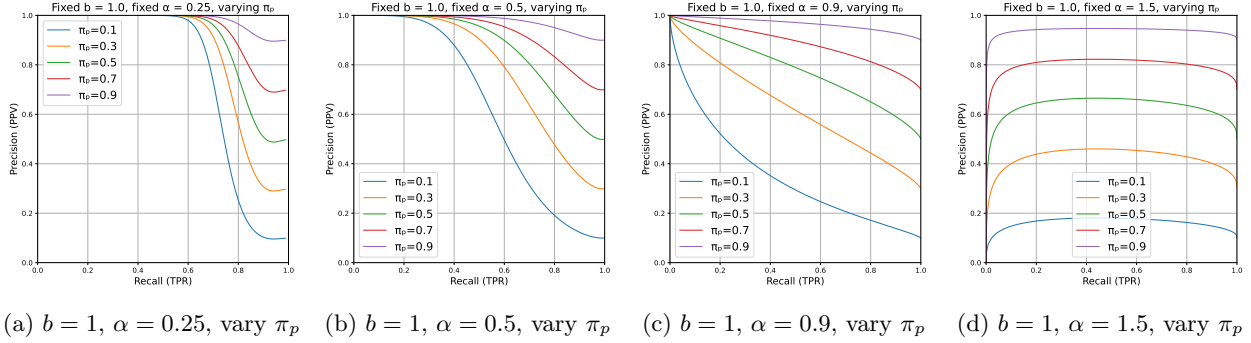


Figure 8: PR curves for binomial positive and negative class scores under fixed values of b and α and varying positive class prevalence ratios.

and varies $\alpha \in \{0.5, 1.0, 1.5, 2.0\}$, demonstrating how dispersion affects PR behavior. The third experiment (Fig. 7c) tests four (α, b) combinations under different class ratios. As expected, increasing class imbalance (i.e., decreasing π_p/π_n) shifts precision downward, even when recall remains high.

Fig. 8 shows other examples where b and α are fixed as π_p varies between $\{0.1, 0.3, 0.5, 0.7, 0.9\}$. We can see the diversity of PR curves.

Appendix

A Proof of AUROC = $\Pr(x_p > x_n)$

We show that the AUROC is equal to the probability that a randomly drawn positive sample point receives a higher score than a randomly drawn negative one (cf. [1, Sec. 2.4]). First,

$$\begin{aligned}
\text{AUROC} &= \int_{-\infty}^{\infty} \text{tpr}(t) d[\text{fpr}(t)] \\
&= \int_0^1 \text{tpr}(\text{fpr}^{-1}(s)) ds \\
&= \int_{-\infty}^{\infty} \text{tpr}(t) f_n(t) dt \\
&= \int_{-\infty}^{\infty} \left[\int_t^{\infty} f_p(x) dx \right] f_n(t) dt \\
&= \int_{-\infty}^{\infty} f_p(x) \left[\int_{-\infty}^x f_n(t) dt \right] dx \\
&= \int_{-\infty}^{\infty} f_p(x) F_n(x) dx \\
&= \Pr(x_p > x_n).
\end{aligned} \tag{45}$$

where we differentiated (6) and a change of variable, to go from the second to the third line. Next, assuming $x_p \sim f_p(x)$ and $x_n \sim f_n(x)$ are independent, we obtain:

$$\begin{aligned}
\Pr(x_p > x_n) &= \iint_{x_p > x_n} f_p(x_p) f_n(x_n) dx_p dx_n \\
&= \int_{-\infty}^{\infty} f_p(x_p) \left[\int_{-\infty}^{x_p} f_n(x_n) dx_n \right] dx_p \\
&= \int_{-\infty}^{\infty} f_p(x) F_n(x) dx.
\end{aligned} \tag{46}$$

B Kullback–Leibler Divergence vs Positive-to-Negative Class Leakage Function

We derive the Kullback–Leibler (KL) divergence between the class-conditional score distributions $f_p(x)$ and $f_n(x)$ using the leakage function $G(u) = F_p(F_n^{-1}(u))$ introduced in (10).

Starting from the standard KL divergence definition:

$$D_{\text{KL}}(f_p \| f_n) := \int_{-\infty}^{\infty} f_p(x) \log \left(\frac{f_p(x)}{f_n(x)} \right) dx, \tag{47}$$

we apply the change of variable $x = F_n^{-1}(u)$, where $u = F_n(x)$, so that

$$dx = \frac{1}{f_n(F_n^{-1}(u))} du.$$

Substituting into the integral gives:

$$D_{\text{KL}}(f_p \| f_n) = \int_0^1 \frac{f_p(F_n^{-1}(u))}{f_n(F_n^{-1}(u))} \log \left(\frac{f_p(F_n^{-1}(u))}{f_n(F_n^{-1}(u))} \right) du. \tag{48}$$

From (10), the derivative of the leakage function is

$$\dot{G}(u) = \frac{f_p(F_n^{-1}(u))}{f_n(F_n^{-1}(u))}.$$

Substituting into the KL expression and combining with (11) yields:

$$D_{\text{KL}}(f_p \| f_n) = \int_0^1 \dot{G}(u) \log \dot{G}(u) du = \int_0^1 g(u) \log g(u) du. \quad (49)$$

which is the negative *differential entropy* of $g(\cdot)$ ¹. This expression relates the information-theoretic divergence between f_p and f_n to the geometric derivative of the leakage function G , which also underlies ROC and PR curve behavior.

Interpretation: The differential entropy of $g(u) = \dot{G}(u)$ provides an interpretable measure of the classifier behavior. The function $g(u)$ captures the rate at which scores of positive sample points leak into the score region corresponding to the u -quantile of the negative class. The differential entropy on the right hand side of (49) quantifies how this leakage is distributed across the decision threshold space. A high entropy value indicates that the classifier’s confusion is spread over a broad range of thresholds, implying misclassifications occur across many regions of the score space. In contrast, a low entropy implies that the leakage is concentrated in a narrow range, suggesting that the classifier generally separates the classes well and only struggles in a localized region. In this way, the entropy of $g(u)$ shows whether the classifier’s errors are widespread and systematic (being generally a poor classifier) or localized and potentially correctable. Since the KL divergence between the positive and negative score distributions is directly related to class separability: lower entropy corresponds to more focused leakage and higher KL divergence, indicating a more discriminative classifier.

Acknowledgment

The author sincerely thanks Dr. Amin Zollanvari from the Department of Electrical and Computer Engineering at Nazarbayev University, and Dr. Matthew A. Reyna from the Department of Biomedical Informatics at Emory University, for their valuable feedback, fruitful discussions and insightful comments on this work.

References

- [1] W. J. Krzanowski and D. J. Hand, *ROC curves for continuous data*. Chapman and Hall/CRC, 2009.
- [2] A. K. Menon and R. C. Williamson, “Bipartite Ranking: a Risk-Theoretic Perspective,” *Journal of Machine Learning Research*, vol. 17, no. 195, pp. 1–102, 2016.
- [3] D. E. Leisman, “Rare Events in the ICU: An Emerging Challenge in Classification and Prediction,” *Critical Care Medicine*, vol. 46, p. 418–424, Mar. 2018.
- [4] H. L. Van Trees, *Detection, estimation, and modulation theory, part I: detection, estimation, and linear modulation theory*. John Wiley & Sons, 2004.
- [5] J. A. Hanley and B. J. McNeil, “The meaning and use of the area under a receiver operating characteristic (ROC) curve,” *Radiology*, vol. 143, p. 29–36, Apr. 1982.
- [6] T. Fawcett, “An introduction to ROC analysis,” *Pattern Recognition Letters*, vol. 27, p. 861–874, June 2006.

¹Remember that $G(\cdot)$ and $g(\cdot)$ are only defined over $[0, 1]$.

- [7] J. Davis and M. Goadrich, “The relationship between Precision-Recall and ROC curves,” in *Proceedings of the 23rd international conference on Machine learning - ICML '06*, ICML '06, p. 233–240, ACM Press, 2006.
- [8] M. A. Reyna, J. Weigle, Z. Koskova, A. Elola, S. Seyedi, K. Campbell, M.-S. Hassannia, J. Pavlus, A. H. Ribeiro, A. L. P. Ribeiro, R. Sameni, and G. D. Clifford, “Detection of Chagas Disease from the ECG: The George B. Moody PhysioNet Challenge 2025,” 2025. Accessed: 2025-04-01.
- [9] D. S. Naidu, *Optimal control systems*. CRC press, 2018.
- [10] R. Sameni, “Model-Based Prediction and Optimal Control of Pandemics by Non-Pharmaceutical Interventions,” *IEEE Journal of Selected Topics in Signal Processing*, vol. 16, p. 307–317, Feb. 2022.
- [11] E. A. Perez Alday, A. B. Rad, M. A. Reyna, N. Sadr, A. Gu, Q. Li, M. Dumitru, J. Xue, D. Albert, R. Sameni, and G. D. Clifford, “Age, sex and race bias in automated arrhythmia detectors,” *Journal of Electrocardiology*, vol. 74, p. 5–9, Sept. 2022.
- [12] M. A. Reyna, Y. Kiarashi, A. Elola, J. Oliveira, F. Renna, A. Gu, E. A. Perez Alday, N. Sadr, A. Sharma, J. Kpodonu, S. Mattos, M. T. Coimbra, R. Sameni, A. B. Rad, and G. D. Clifford, “Heart murmur detection from phonocardiogram recordings: The George B. Moody PhysioNet Challenge 2022,” *PLOS Digital Health*, vol. 2, p. e0000324, Sept. 2023.
- [13] E. A. Perez Alday, A. Gu, A. J Shah, C. Robichaux, A.-K. Ian Wong, C. Liu, F. Liu, A. Bahrami Rad, A. Elola, S. Seyedi, Q. Li, A. Sharma, G. D. Clifford, and M. A. Reyna, “Classification of 12-lead ECGs: the PhysioNet/Computing in Cardiology Challenge 2020,” *Physiological Measurement*, vol. 41, p. 124003, Dec. 2020.
- [14] A. Papoulis and S. U. Pillai, *Probability, Random Variables and Stochastic Processes*. McGraw-Hill, 4th ed., 2002.